Supporting information for

Therapeutic mesopore construction on 2D Nb_2C MXenes for targeted and enhanced chemo-photothermal cancer therapy in NIR-II biowindow

Xiaoxia Han[1], Xiangxiang Jing[2]*, Dayan Yang[2], Han Lin[3], Zhigang Wang[1], Haitao Ran[1], Pan Li[1]* and Yu Chen[3]*

[1]Chongqing Key Laboratory of Ultrasound Molecular Imaging, Ultrasound Department of the Second Affiliated Hospital of Chongqing Medical University. Chongqing, 400010, P. R. China.

[2]Department of Ultrasound, Hainan General Hospital, Haikou, 570311, P. R. China.

[3]State Key Laboratory of High Performance Ceramics and Superfine Microstructure, Shanghai Institute of Ceramics, Chinese Academy of Sciences, Shanghai, 200050, P. R. China.

E-mail: cqlipan@163.com (P. Li); ljjxx2000@126.com (X. Jing); chenyu@mail.sic.ac.cn (Y. Chen)

Calculation of extinction coefficient and photothermal-conversion efficiency

a. Calculation of extinction coefficient

The extinction coefficient ε(λ) was acquired to evaluate the NIR-II absorption potential, and the ε(λ) was analyzed based on Lambert-Beer law:

$$A(\lambda) = \varepsilon LC \quad (1)$$

where A is the absorbance of CTAC@Nb_2C-MSN at the wavelength of λ, L means the length of test tube (1 cm) and C represents the Nb concentration of CTAC@Nb_2C-MSN nanoparticles. The slope of the linear fit between wavelength and absorbance gives the extinction coefficient of CTAC@Nb_2C-MSN at 1064 nm which is 9.71 $g^{-1}cm^{-1}$.

b. Calculation of photothermal-conversion efficiency

The energy of whole system meets the following balance formula:

$$\sum_i m_i C_{p,i} \frac{dT}{dt} = Q_{Sam} + Q_{Dis} - Q_{Env} \quad (2)$$

where m represents the weight of water solution (0.3 g) and C means specific heat capacity of water (4.2J/(g·K)), T is the temperature of CTAC@Nb_2C-MSN, and Q_{Sap} represents input energy of CTAC@Nb_2C-MSN nanoparticles, Q_{Dis} means the input energy produced by test tube, Q_{Env} represents the heating energy produced by the whole system which released to the air.

According to following formula, CTAC@Nb_2C-MSN nanosystem-assisted heating procedure depends on surface plasmon electron-phonon relaxation irradiated by 1064 nm laser:

$$Q_{Sam} = I(1 - 10^{-A_{1064}})\eta \quad (3)$$

where I means the incident laser energy of 1064 nm laser (mW), A_{1064} is the absorbance of

CTAC@Nb_2C-MSN at the wavelength of 1064 nm. η represents photothermal-conversion efficiency of noanosystems from incident energy to thermal energy.

In addition, Q_{Dis} means the heat dissipated from the sample tube. It was analyzed by measuring the temperature fluctuations of water solution in cell. Definitively, Q_{Dis} was determined to be $(5.4\times10^{-4})I$. Q_{Env} tended to measure linearly with the output energy:

$$Q_{Env} = hS(T - T_{Env}) \tag{4}$$

where h means heat transfer coefficient and S is the surface area of the system. T means the surface temperature of heating pocket and T_{Env} is the outside temperature.

The heat input energy (Q_{Sam} + Q_{Dis}) of the system is limited when 1064 nm laser power is defined. The relationship between the output energy (Q_{Env}) changing with the temperature of system is positive correlation, and the temperature of whole system would get to the peak when the heat energy is equal to heat energy.

$$Q_{Sam} + Q_{Dis} = Q_{Env-Max} = hS(T_{Max} - T_{Env}) \tag{5}$$

$Q_{Env\text{-}Max}$ represents the operating energy escape from the heating system *via* air when the sample cell reaches to the equalization temperature. T_{Max} represents the temperature which means no heat escape away from the system. Furthermore, substituting Eq. (3) into Eq. (5), we obtain Eq. (6) as follows:

$$\eta = \frac{hS(T_{Max} - T_{Env}) - Q_{Dis}}{I(1 - 10^{-A_{1064}})} \tag{6}$$

where A_{1064} is the absorbance of CTAC@Nb_2C-MSN at the wavelength of 1064 nm. To calculate the hS, θ is introduced and means for

$$\theta = \frac{T - T_{Env}}{T_{Max} - T_{Env}} \tag{7}$$

then time constant of the whole system can be described as:

$$\tau_S = \frac{\sum_i m_i C_{p,i}}{hS} \tag{8}$$

Followed substituting (8) to (2) and got the following transformation,

$$\frac{\mathrm{d}\theta}{dt} = \frac{1}{\tau_s}\left[\frac{Q_{Sam} + Q_{Dis}}{hS(T_{Max} - T_{Env})} - \theta\right] \tag{9}$$

In the cooling period of CTAC@Nb_2C-MSN, $Q_{Sam} + Q_{Dis} = 0$, so after being substitued to (9) and transferred,

$$dt = -\tau_s \frac{d\theta}{\theta} \tag{10}$$

After being rearranged, the following formula is got:

$$t = -\tau_s In\theta \tag{11}$$

Then, time constant of heat transfer from the whole system is calculated to 180.22s of 1064 nm (**Figure 4i**). Finally, hS can be calculated by (8), and laser photothermal conversion efficiency (η) of CTAC@Nb_2C-MSN nanoparticles is calculated to be 28.6%.

Supplementary figures and discussion

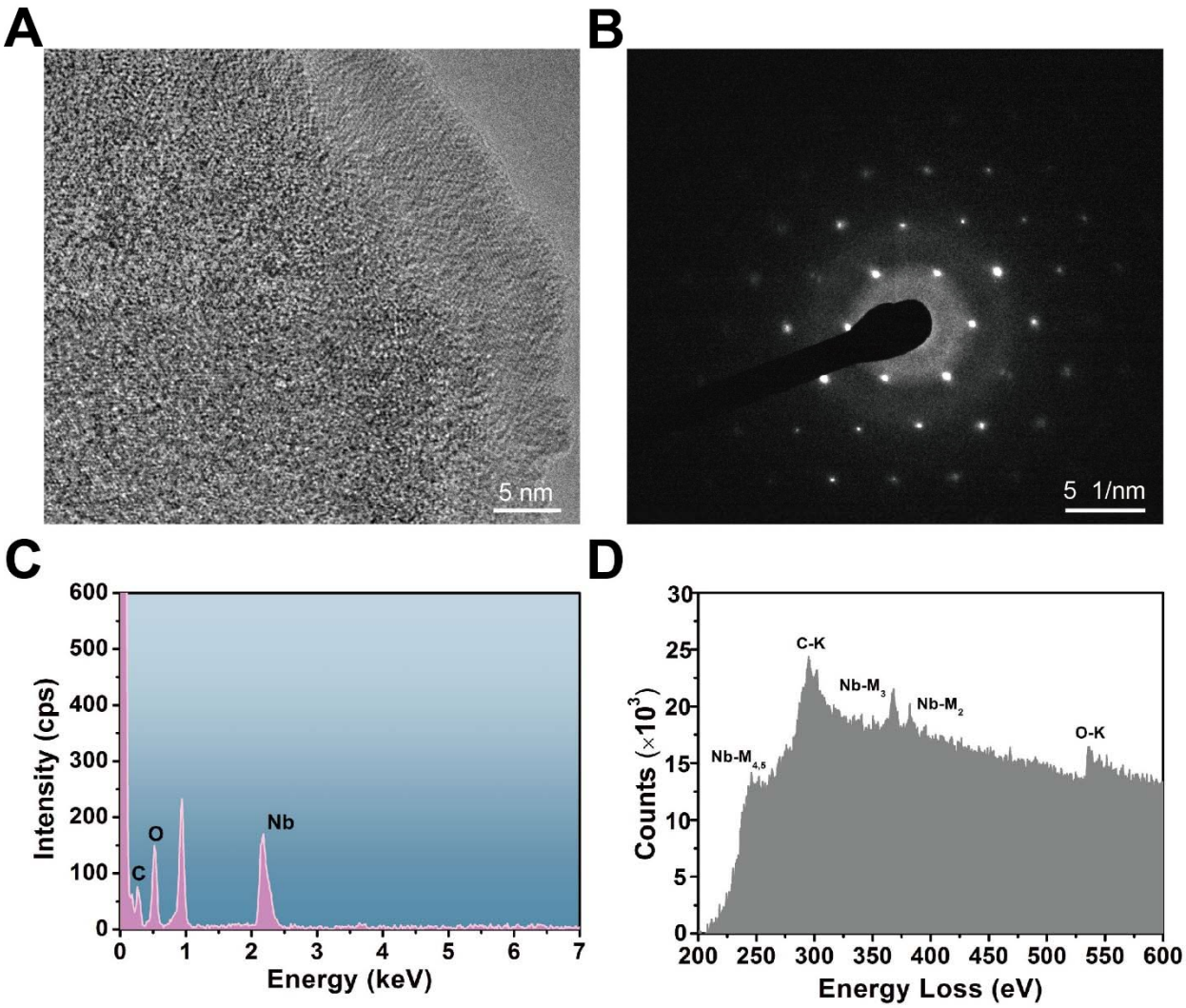

Figure S1. (A) High-solution TEM (HRTEM) image of 2D Nb_2C MXene and (B) corresponding selected area electron diffraction (SAED). (C) energy dispersive spectrum (EDS) and (D) electron energy loss spectroscopy (EELS) of 2D Nb_2C MXene.

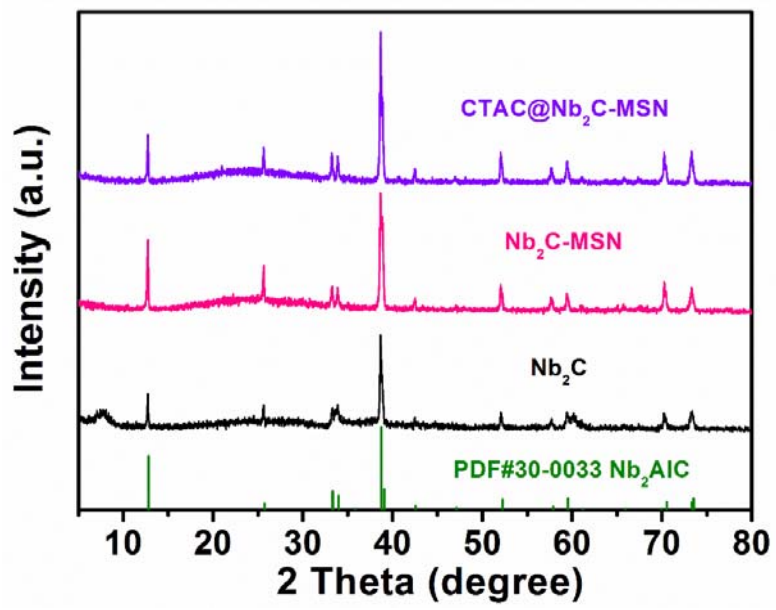

Figure S2. X-ray diffraction (XRD) patterns of Nb_2C, Nb_2C-MSN and CTAC@Nb_2C-MSN.

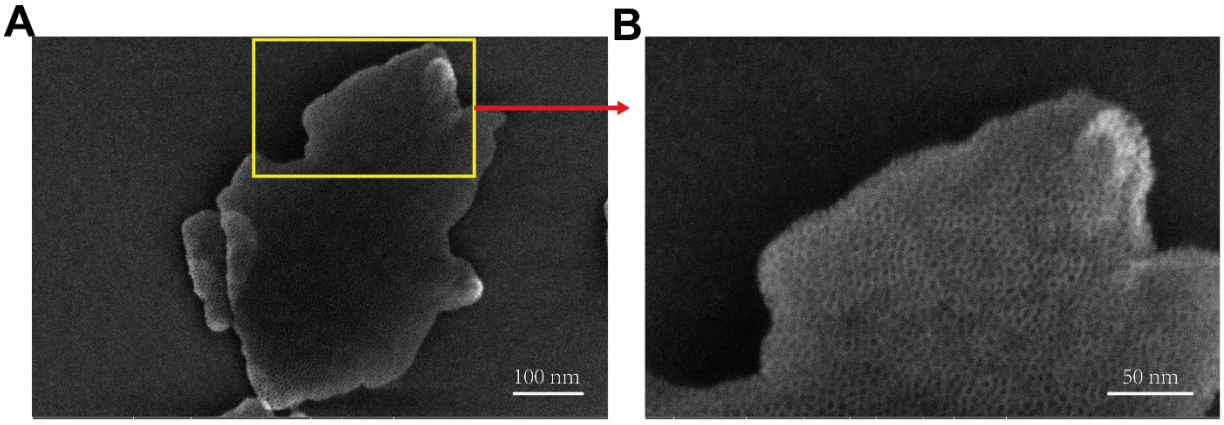

Figure S3. (A) Low magnification and (B) high resolution SEM images of CTAC@Nb_2C-MSN composite nanosheets.

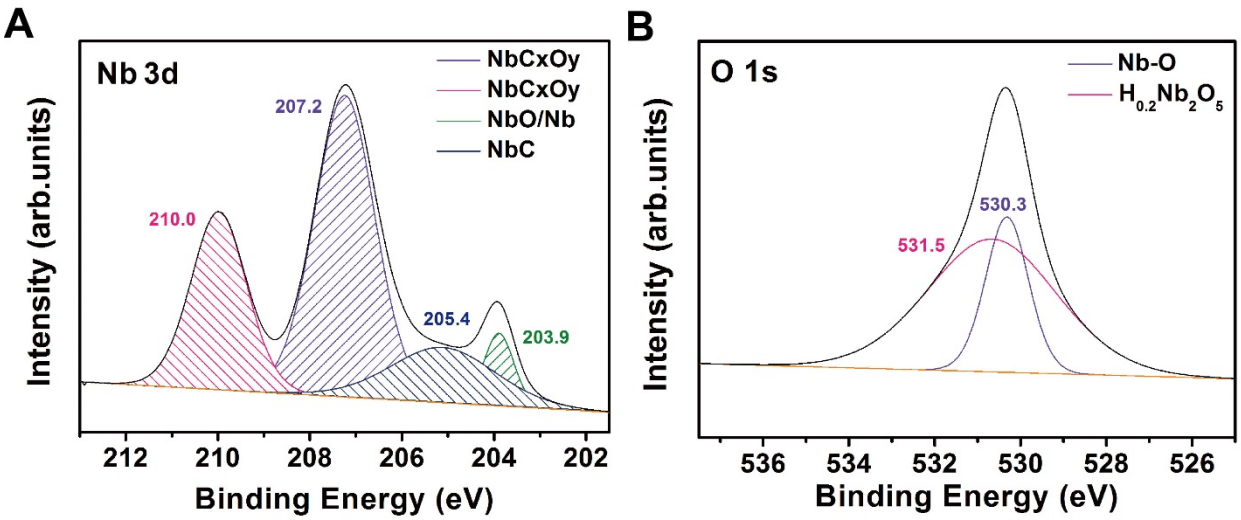

Figure S4. XPS spectra of Nb_2C in Nb 3d (A) O 1s (B) region.

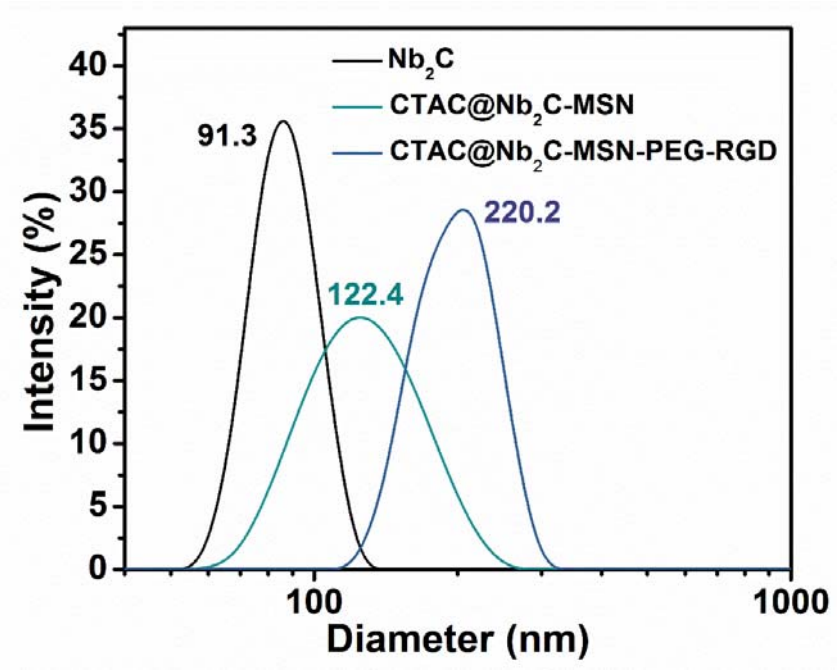

Figure S5. Dynamic light scattering (DLS) size distribution of Nb_2C, CTAC@Nb_2C-MSN and CTAC@Nb_2C-MSN-PEG-RGD.

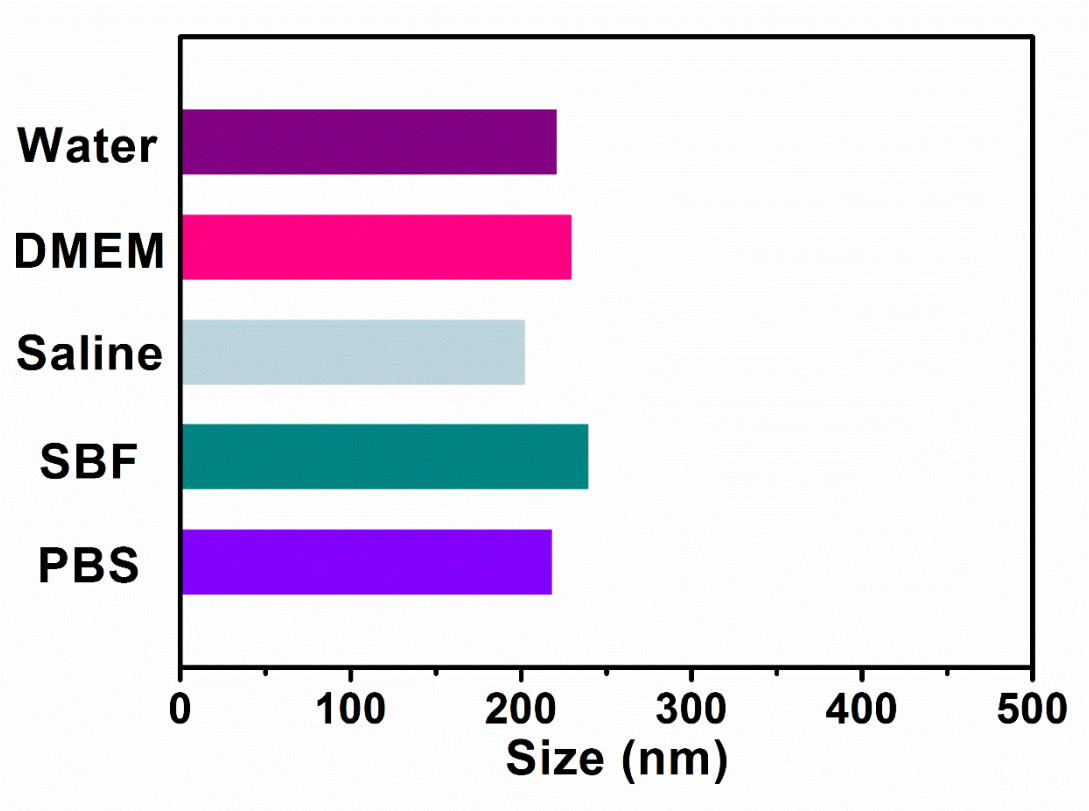

Figure S6. The average particle size of CTAC@Nb_2C-MSN-PEG-RGD in different solvents (Water, DMEM, Saline, SBF and PBS) as determined by dynamic light scattering (DLS).

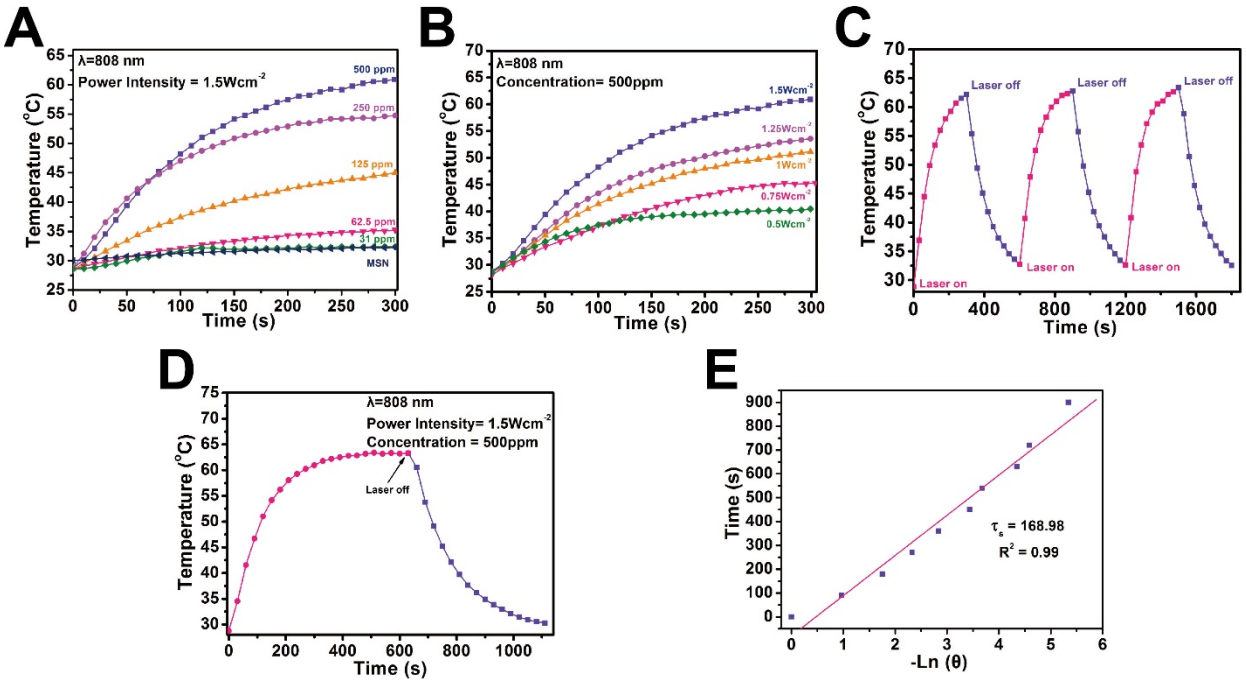

***Figure S7. In vitro* photothermal-conversion assessment of CTAC@Nb_2C-MSN in NIR-I biowindow.** (A) The temperature changes of CTAC@Nb_2C-MSN aqueous solution with the prolonged NIR-I laser (808 nm, power density: 1.5 W cm^{-2}) irradiation duration at elevated concentrations (31, 61.5, 125, 250 and 500 μg/mL). (B) Photothermal-heating curves of CTAC@Nb_2C-MSN dispersed in aqueous solution irradiated by different power intensities (0.5, 0.75, 1.0, 1.25 and 1.5 W cm^{-2}) of NIR-I laser at the wavelength of 808 nm. (C) Heating curve of CTAC@Nb_2C-MSN dispersed in water for three laser on/off cycles irradiated by 808 nm laser at the power intensity of 1.5 W cm^{-2}. (D) Photothermal performance of CTAC@Nb_2C-MSN dispersed in aqueous solution under the 808 nm laser irradiation, and the laser was turn off when the temperature was stable. (E) Time constant for heat process transfer calculated from the cooling period.

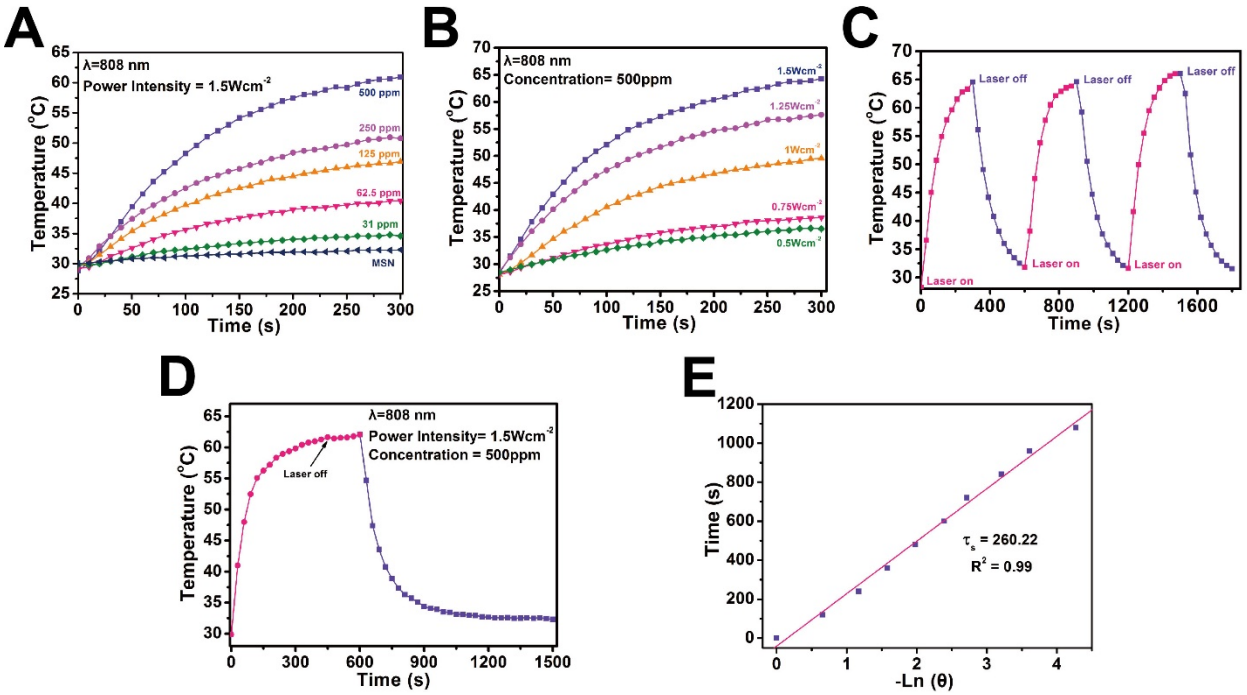

***Figure S8. In vitro* photothermal-conversion assessment of Nb_2C in NIR-I biowindow.** (A) The temperature changes of Nb_2C aqueous solution with the prolonged NIR-I laser (808 nm, power density: 1.5 W cm^{-2}) irradiation duration at elevated concentrations (31, 61.5, 125, 250 and 500 μg/mL). (B) Photothermal-heating curves of Nb_2C dispersed in aqueous solution irradiated by different power intensities (0.5, 0.75, 1.0, 1.25 and 1.5 W cm^{-2}) of NIR-I laser at the wavelength of 808 nm. (C) Heating curve of CTAC@Nb_2C-MSN dispersed in water for three laser on/off cycles irradiated by 808 nm laser at the power intensity of 1.5 W cm^{-2}. (D) Photothermal performance of Nb_2C dispersed in aqueous solution under the 808 nm irradiation, and the laser was turn off when the temperature was stable. (E) Time constant for heat process transfer calculated from the cooling period.

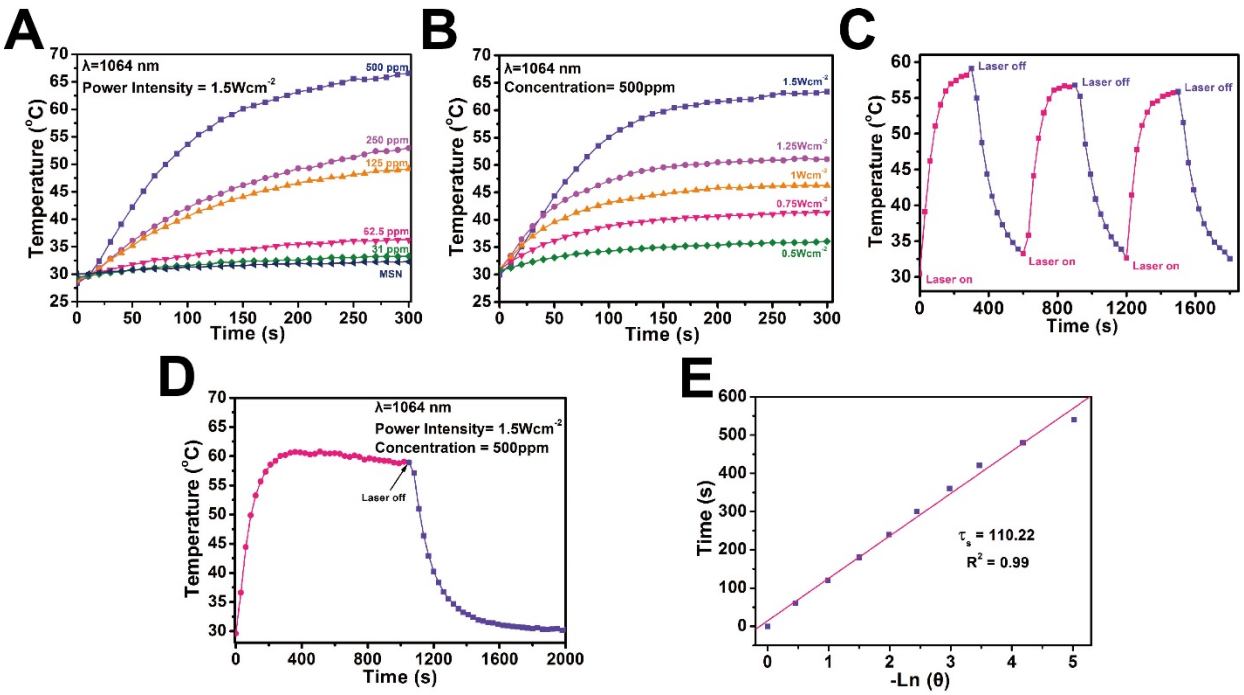

***Figure S9. In vitro* photothermal-conversion assessment of Nb_2C in NIR-Ⅱ biowindow.** (A) The temperature changes of Nb_2C aqueous solution with the prolonged NIR-II laser (1064 nm, power density: 1.5 W cm^{-2}) irradiation duration at elevated concentrations (31, 61.5, 125, 250 and 500 μg/mL). (B) Photothermal-heating curves of Nb_2C dispersed in aqueous solution irradiated by different power intensities (0.5, 0.75, 1.0, 1.25 and 1.5 W cm^{-2}) of NIR-I laser at the wavelength of 1064 nm. (C) Heating curve of CTAC@Nb_2C-MSN dispersed in water for three laser on/off cycles irradiated by 1064 nm laser at the power intensity of 1.5 W cm^{-2}. (D) Photothermal performance of Nb_2C dispersed in aqueous solution under the 1064 nm irradiation, and the laser was turn off when the temperature was stable. (E) Time constant for heat process transfer calculated from the cooling period.

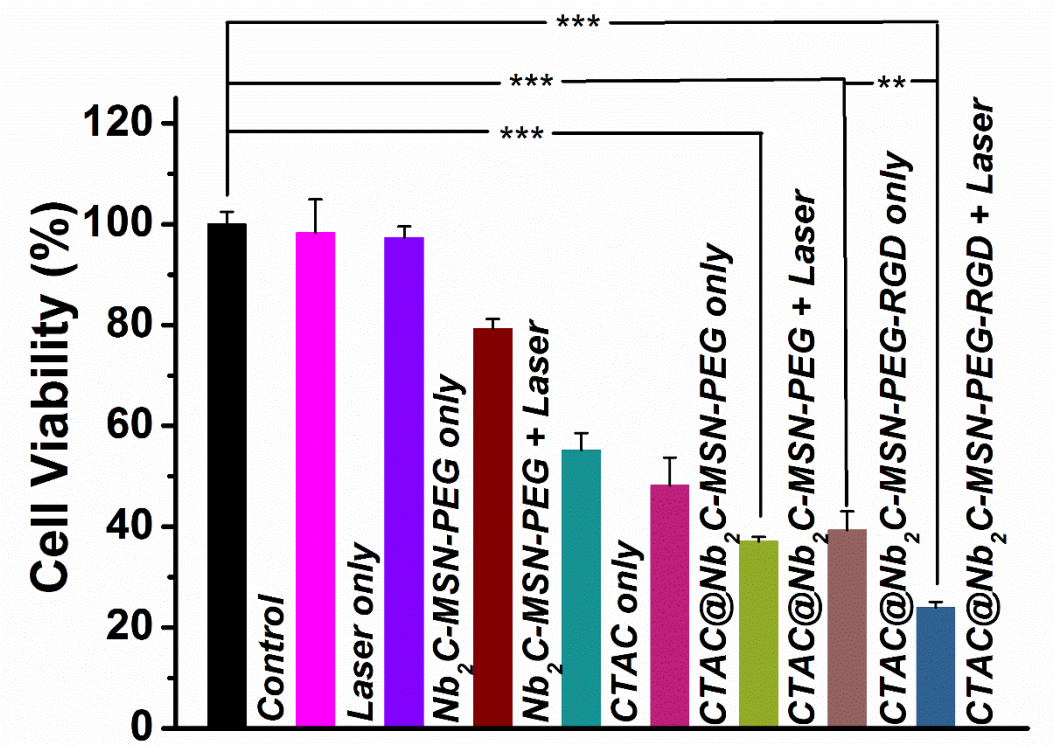

Figure S10. Relative cell viability of U87 cells after different treatments, including control (without treatment), Laser only, Nb_2C-MSN-PEG only, Nb_2C-MSN-PEG combined with laser irradiation, CTAC only group, CTAC@Nb_2C-MSN-PEG only, CTAC@Nb_2C-MSN-PEG combined with laser irradiation, CTAC@Nb_2C-MSN-PEG-RGD only, CTAC@Nb_2C-MSN-PEG-RGD combined with laser irradiation (1064 nm laser, 1 $W \cdot cm^{-2}$) (**P < 0.01, ***P < 0.001).

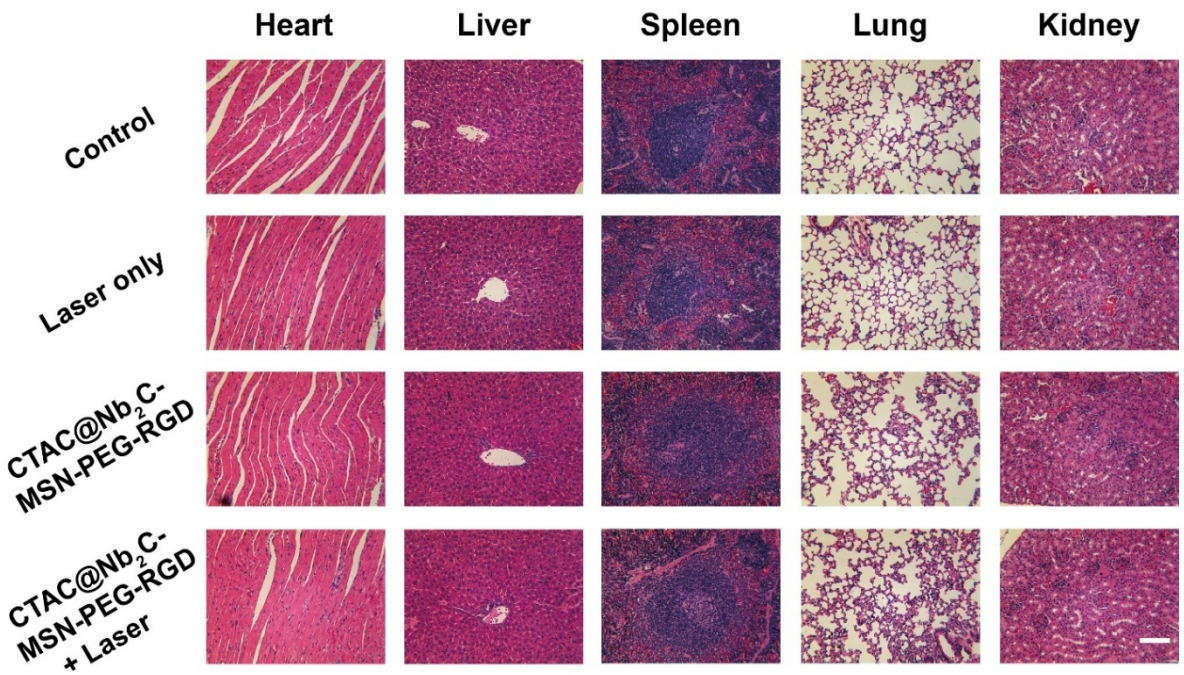

Figure S11. H&E-staining of major organs (heart, liver, spleen, lung and kidney) from U87-bearing nude mice after 1d's various treatments (control (without treatment), Laser only, CTAC@Nb_2C-MSN-PEG-RGD only, CTAC@Nb_2C-MSN-PEG-RGD combined with laser irradiation (1064 nm laser). Scale bar: 20 μm.

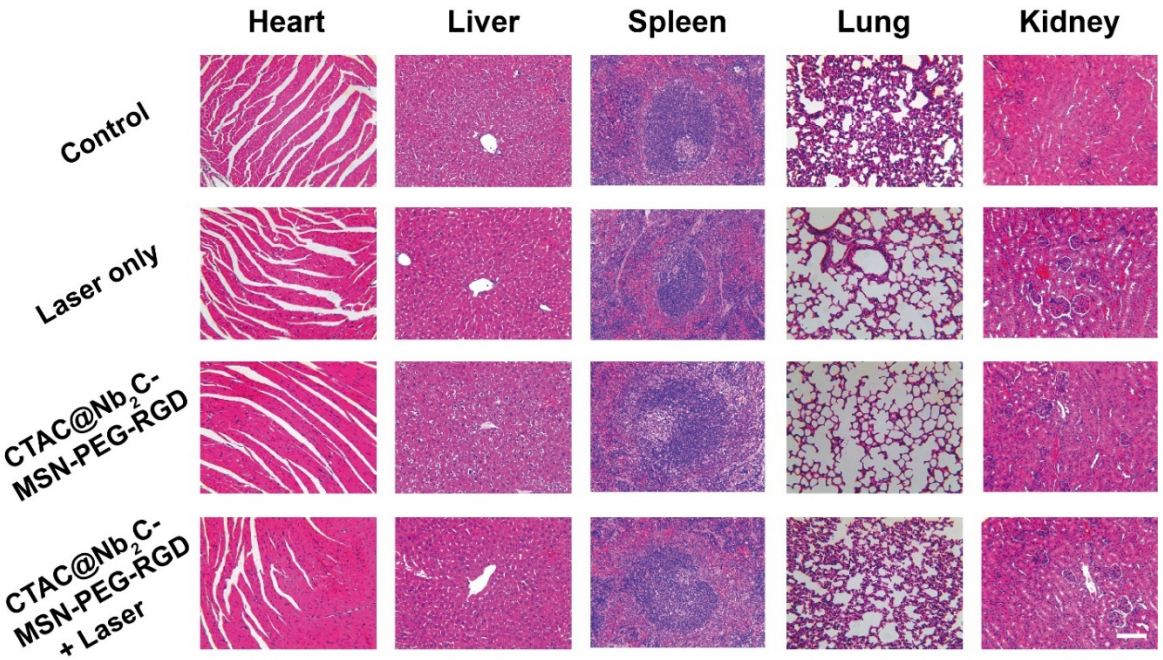

Figure S12. H&E-staining of major organs (heart, liver, spleen, lung and kidney) from U87-bearing nude mice after 15d's various treatments (control (without treatment), Laser only, CTAC@Nb_2C-MSN-PEG-RGD only, CTAC@Nb_2C-MSN-PEG-RGD combined with laser irradiation (1064 nm laser). Scale bar: 20 μm.

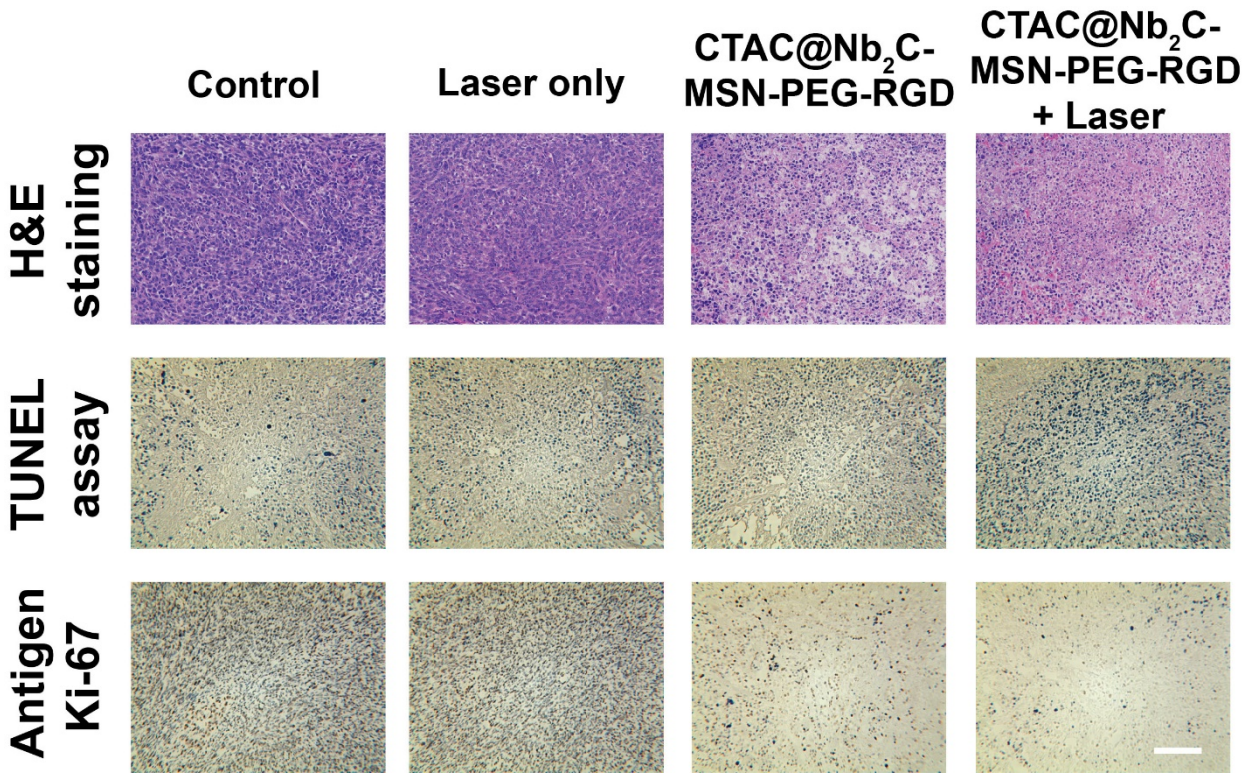

Figure S13. H&E staining, TUNEL staining and Antigen Ki-67 immunofluorescence staining in tumor region of each group after 1d's treatments. Scale bar: 50 μm.